

学位論文（要約）

A study on the structure of tornado-spawning typhoons

（竜巻を生ずる台風の構造に関する研究）

平成 28 年 12 月博士（理学）申請

東京大学大学院理学系研究科

地球惑星科学専攻

末木 健太

## Abstract

The structure of typhoons that spawned tornadoes (tornadic typhoons: TTs) in Japan from 1991 to 2013 were investigated by composite analysis using Japanese 55-year Reanalysis and compared with that of typhoons that did not spawn tornadoes (non-tornadic typhoons: NTs). Two environmental parameters, storm-relative environmental helicity (SREH) and convective available potential energy (CAPE), which give potential of supercells, were examined.

SREH is large in the northeast quadrant of TTs, where tornado occurrences were concentrated, and SREH in that quadrant for TTs is significantly larger than that for NTs, indicating that the structure of TTs is favorable to supercell generation. Larger SREH for TTs can be attributed to larger vertical veering shear in the northeast quadrant, which was caused by stronger intensity of the typhoon and larger synoptic-scale vertical wind shear superposed on the typhoon vortex. Faster synoptic-scale wind speed at the mid-troposphere that increases the propagation speeds of supercells also contributes to larger SREH for TTs. TTs are also more strongly affected by the synoptic-scale baroclinicity, so that the index of cyclone's symmetry,  $B$ , is significantly larger than that for NTs. In fact, a majority of TTs satisfy the criterion for the onset of extratropical transition ( $B > 10$  m).

Two kinds of CAPE were examined: one is ordinary CAPE which does not consider the effects of entrainment, and the other is entraining CAPE (E-CAPE). The ordinary CAPE is large in the southeast of the typhoon center, and does not explain the distribution of the tornadoes in the northeast quadrant. On the other hand, E-CAPE is found to be large in the northeast quadrant of both TTs and NTs, and its value for TTs is significantly larger than that for NTs. Thus, E-CAPE is a good indicator of potential risk

for typhoon-associated tornadoes. Larger E-CAPE for TTs was caused by a larger temperature lapse rate in the mid-troposphere. Time series analysis in addition to the composite analysis implies that an entrainment rate of about  $20\% \text{ km}^{-1}$  gives the most appropriate E-CAPE: E-CAPE for this value of entrainment rate increases its value right before the tornadogenesis and rapidly decreases after it.

In order to confirm if the entrainment rate of about  $20\% \text{ km}^{-1}$  is a reasonable estimate for a typhoon-associated tornado environment, a large eddy simulation was performed for a horizontally homogeneous basic-state based on the observed sounding in the northeast quadrant of a tornado-spawning typhoon (Typhoon 9018). The simulation successfully reproduced a storm which had typical characteristics of typhoon-associated supercells. For the purpose of estimating entrainment rates in the simulated supercell, a steady-state one-dimensional entraining plume model was assumed, where the plume is defined as a continuous updraft region in which vertical velocity exceeds  $5 \text{ m s}^{-1}$ . The basic state also has a passive tracer whose concentration decreases linearly with increasing height. It is found that the entraining plume model with a constant entrainment rate gives a reasonable approximation to the simulated distribution of the passive tracer concentration for the layer from the top of the boundary layer to the mid-troposphere. In this layer, an entrainment rate was estimated to be about  $15\text{--}20\% \text{ km}^{-1}$ , which is consistent with the assumed entrainment rate used in the E-CAPE calculation. Above the altitude of about 6 km, on the other hand, the entraining plume model seems to be no longer appropriate because substantial detrainment occurs. The entrainment rate of  $20\% \text{ km}^{-1}$  in the E-CAPE calculation turns out to be physically reasonable value at least up to the mid-troposphere.

The present study suggests that a suitable combination of SREH and E-CAPE is

capable for better assessment of tornado potential associated with tropical cyclones. Furthermore, E-CAPE may be a useful parameter in assessing tornado potential in other environments that are not associated with tropical cyclones.

# Contents

<b>1. General Introduction</b> .....	1
1.1. Supercell formation and tornadogenesis.....	2
1.2. Environmental parameters for assessing tornado potential.....	8
1.3. Tornadoes spawned by tropical cyclones .....	12
1.4. Purpose of this thesis .....	15
<b>2. Statistical Characteristics of Tornado-spawning Typhoons</b> .....	16
2.1. Introduction .....	16
2.2. Data and methods .....	17
2.2.1. Data sources and targets of analysis .....	17
2.2.2. Method of composite analysis .....	19
2.2.3. Method of time series analysis .....	21
2.3. Analysis of SREH.....	21
2.3.1. Calculation of SREH .....	21
2.3.2. Composite distribution and time series .....	22
2.3.3. Factors contributing to larger SREH of TTs.....	23
2.3.4. Interpretation by cyclone phase space .....	36
2.4. Analysis of CAPE.....	41
2.4.1. Calculation of CAPE .....	41
2.4.2. Composite distribution and time series .....	42
2.4.3. Impacts of entrainment on the distribution of CAPE .....	43
2.4.4. Main factor contributing to larger E-CAPE of TTs .....	46
2.4.5. Sensitivity to entrainment rate .....	48
2.5. Discussion.....	50
2.5.1. Complementary contributions of SREH and E-CAPE.....	50
2.5.2. Tornadoes in the Okinawa District .....	55
2.5.3. Interpretation of “non-tornadic” typhoons .....	57
2.6. Summary and conclusions .....	61
<b>3. Large Eddy Simulations for Estimating Entrainment Rates of Typhoon-associated Supercells</b> .....	63
3.1. Introduction .....	63

3.2.	Model and experimental design.....	67
3.2.1.	Model settings .....	67
3.2.2.	Experimental design .....	67
3.2.3.	Environmental profile.....	69
3.3.	Overview of the simulated supercell .....	70
3.3.1.	Time evolution of the supercell .....	70
3.3.2.	Supercell movement .....	75
3.3.3.	Tornadogenesis .....	77
3.3.4.	Summary.....	83
3.4.	Method for estimating entrainment rate .....	83
3.4.1.	Passive tracer .....	83
3.4.2.	Updraft plume.....	86
3.4.3.	Entraining plume model .....	88
3.5.	Results .....	92
3.5.1.	Vertical distribution of passive tracer concentration in the updraft plume	92
3.5.2.	Estimation of the entrainment rate.....	93
3.6.	Discussion.....	97
3.7.	Summary and conclusions .....	99
<b>4.</b>	<b>General Conclusions and Future Perspectives .....</b>	<b>101</b>
	<b>Acknowledgments.....</b>	<b>104</b>
	<b>References.....</b>	<b>105</b>

# 1. General Introduction

Tornadoes are the most violent small-scale vortices in the atmosphere which can cause serious human and property damage. According to the National Weather Service, 70 people per year on average are killed by the tornadoes in the US between 1986 and 2015. Thus, investigations of the tornadoes and their environment are important for both the development of meteorology and the disaster prevention. While the observation or the forecasting of tornadoes is still a challenge, the accumulation of the past tornado data and the recent release of accurate reanalysis data of the atmosphere have advanced both statistical studies of the tornado events and investigation of the environmental conditions favorable to tornado occurrences.

In Japan, a significant fraction (20%) of tornadoes is spawned by typhoons (Niino et al., 1997), which are defined as tropical cyclones (TCs) having a maximum wind larger than  $17 \text{ m s}^{-1}$  over the northwestern Pacific Ocean. The tornado associated with Typhoon 9918 in Toyohashi City, Aichi Prefecture, on 24 September, was one of the most intense tornadoes that occurred in Japan (F3 in the Fujita scale:  $70\text{--}90 \text{ m s}^{-1}$ ) and damaged more than 2,300 houses. The F2 ( $50\text{--}69 \text{ m s}^{-1}$ ) tornado associated with Typhoon 0613 in Nobeoka City, Miyazaki Prefecture, on 17 September killed three people, which motivated Japan Meteorological Agency (JMA) to upgrade 20 conventional radars to Doppler radars. Recently, Typhoon 1318 produced 11 tornadoes from Wakayama to Miyagi Prefectures, which was one of the unusual tornado outbreaks in Japan. Thus, understanding of typhoon-spawned tornadoes is important for meteorology and disaster mitigation in Japan. The United States also experiences significant tornado outbreaks associated with TCs (see section 1.3).

This chapter consists of three sections: In section 1.1, the basic understanding of

tornadoes and their parent convective clouds called “supercells” is reviewed briefly, because typhoon-associated tornadoes are also known to be spawned by a certain class of supercells. In section 1.2, some important environmental parameters for assessing the tornado potential, which are to be mainly used for the present analysis, are explained. In section 1.3, previous studies on tornadoes associated with TCs are reviewed. Finally, the motivation for this thesis is presented in section 1.4.

## **1.1. Supercell formation and tornadogenesis**

Most of intense tornadoes are known to be generated by supercells (Davies-jones et al., 2001). In general, a supercell is defined as a long-lived convective storm having a rotating updraft called a mesocyclone whose vertical vorticity is greater than  $0.01 \text{ s}^{-1}$ . The word “supercells” was first coined by Browning (1964) who proposed a conceptual model of the storm characterized by its rightward deviating motion relative to the tropospheric mean winds. Previous studies have clarified that such rightward deviating characteristics is essential to the formation of the mesocyclone in the supercell.

The necessary condition for the supercell formation is a strong vertical wind shear of the environment in addition to a conditionally unstable atmosphere (Weisman and Klemp, 1982). By using a three-dimensional cloud model, Wilhelmson and Klemp (1978) successfully simulated a long-lived rotating convective cloud in the environment of a unidirectional westerly vertical wind shear. In such an environment, an initial updraft triggered by a thermal bubble generates a vortex pair consisting of a cyclonic vortex on the south and an anticyclonic vortex on the north, by tilting a horizontal vortex tube associated with the environmental vertical shear (Fig. 1-1a). As precipitation starts near the center of the updraft, the precipitation-associated downdraft splits the

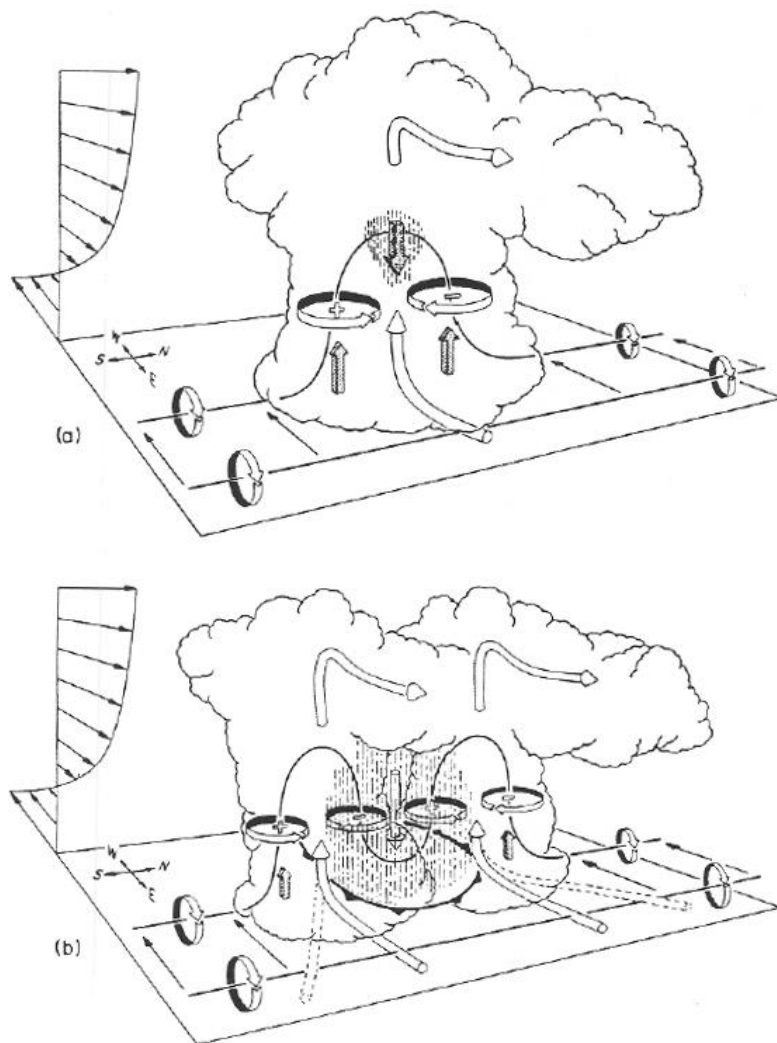


**Fig. 1-1.** Conceptual model of an early development stage of right- and left-moving supercells in the environment of a unidirectional (east–west) vertical wind shear. (a) shows initial generation of vertical vorticity in the mid-troposphere due to tilting of horizontal vorticity of environmental winds. (b) shows a splitting of the storm due to the precipitation associated downdraft. (From Klemp, 1987.)

storm into two parts: one is in the southern side and the other is in the north side (Fig. 1-1b). Since a warm moist low-level air is supplied from the east relative to the eastward-moving storms, dynamically induced upward pressure gradient forces under the southern mesocyclone and northern meso-anticyclone help the storms maintain continuously. The cyclonically rotating updraft on the south side continuously propagates southeastward (right to the mid-level environmental wind) and the northern

anticyclonic one propagates northeastward (left to the environmental wind), where they are referred to as right- and left-moving supercells, respectively.

Both right- and left-moving supercells can develop in the unidirectional shear environment, whether the Coriolis effect is considered or not (Klemp and Wilhelmson, 1978b). However, if the environmental wind has a veering vertical shear as shown in the hodograph of Fig. 1-2, only the right-moving storm can be intensified. By using a linear theory, Rotunno and Klemp (1982) proposed that dynamical pressure perturbations due to the interaction between the environmental vertical shear and the storm updraft work favorably for the right mover in the veering shear environment. According to their theory, a positive (negative) pressure perturbation is generated on the upshear (downshear) side of the updraft center with respect to the environmental vertical shear vector. In a unidirectional shear environment, the resulting upward (downward) pressure gradient force, which enhances (suppresses) the convective updraft, exists on the east (west) side of the storm (Fig. 1-3a). However, since the pressure gradient forces act equally on both the southern and northern storms, no difference in the development of

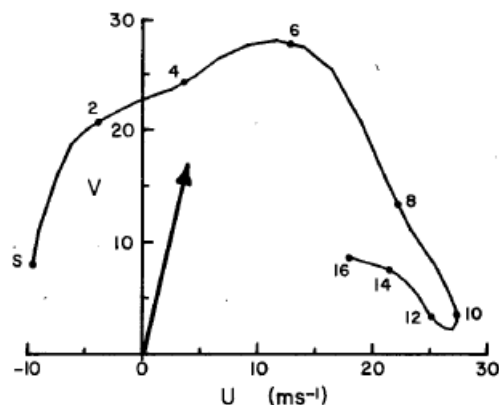


**Fig. 1-2.** Environmental wind hodograph for the cyclonically rotating right-moving supercell occurred at Del City, Oklahoma on 20 May 1977. The arrow represents the observed propagation speed of the supercell. (From Klemp et al., 1981.)

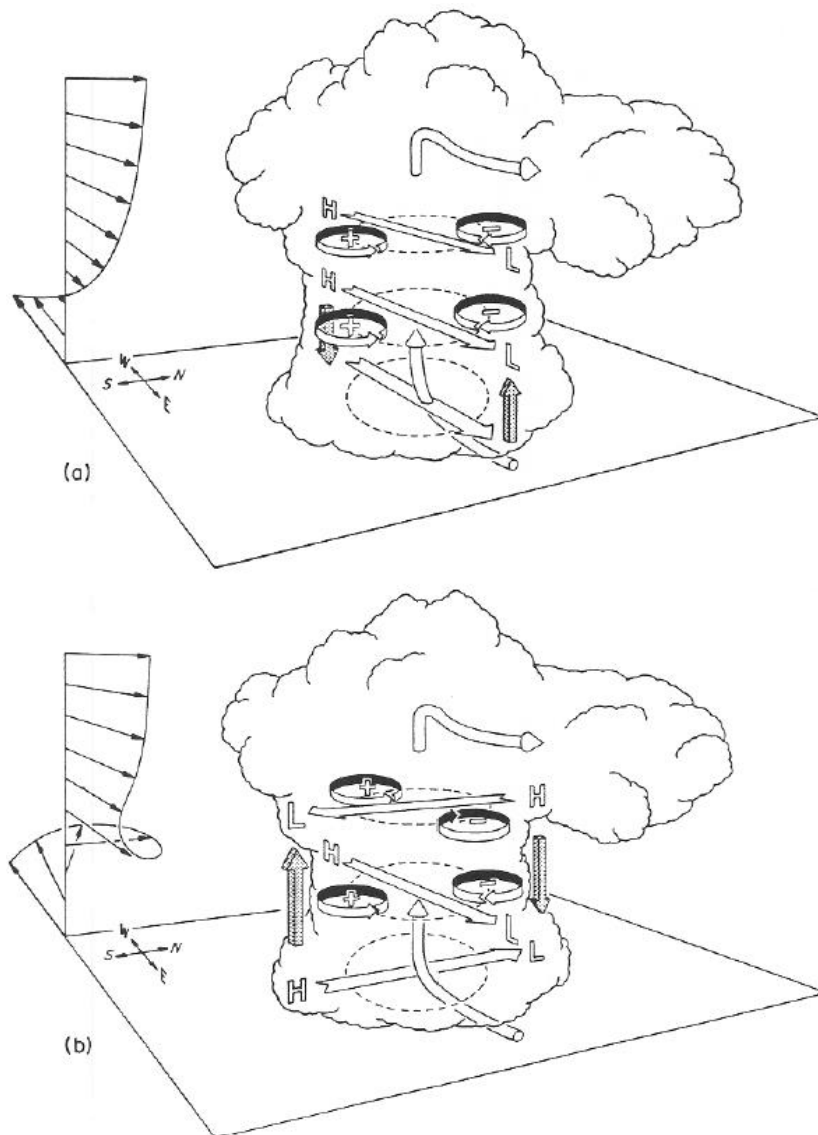


**Fig. 1-3.** Schematic illustration of the dynamical pressure perturbations due to the interaction between the environmental wind shear and the storm updraft, and resulting vertical pressure gradient forces. (a) shows the storm developed in the unidirectional westerly vertical shear and (b) shows that for the vertically veering shear. The flat arrows represent the shear vectors of the environment for each height. Labels H and L represent positive and negative pressure perturbations, respectively. The shaded arrows represent the directions of vertical pressure gradient forces. (From Klemp, 1987.)

the both storms occurs. On the other hand, in a veering shear environment, upward (downward) pressure gradient force occurs on the south (north) side of the convection, because the lower-level shear vector is oriented to the north and the upper-level shear

vector is oriented to opposite direction (Fig. 1-3b). Thus, the development of the right-moving (left-moving) supercell on the south (north) side is enhanced (suppressed). In the Northern Hemisphere, most of observed supercells are the right movers, because an environmental wind generally turns clockwise with increasing height.

The cyclonically rotating supercells in the quasi-steady state continue to propagate to the right of the environmental wind, which can be attributed to the upward pressure gradient force due to the mid-level mesocyclone whose center of the rotation is located at the right of the updraft center. On the other hand, this rightward propagation is also necessary for the cyclonic rotation in the updraft (e.g., Davies-jones, 1984; Lilly 1986). According to the linear theory developed by Davies-jones (1984), the generation of net cyclonic vorticity in the updraft through tilting requires environmental storm-relative streamwise vorticity  $\omega_s$ :

$$\omega_s = \frac{(\vec{V}_h - \vec{C}) \cdot \left( \vec{k} \times \frac{\partial \vec{V}_h}{\partial z} \right)}{|\vec{V}_h - \vec{C}|}, \quad (1.1)$$

where  $\vec{V}_h$  is the horizontal wind vector,  $\vec{C}$  is the storm motion vector, and  $\vec{k}$  is the unit vector in the vertical direction.  $\vec{V}_h - \vec{C}$  and  $\vec{k} \times \partial \vec{V}_h / \partial z$  represent the storm-relative wind and the horizontal vorticity associated with the environmental vertical wind shear, respectively. On the other hand, crosswise vorticity (the component of the horizontal vorticity perpendicular to the storm-relative wind direction) does not contribute to net cyclonic rotation of the updraft. The right-moving supercell can obtain abundant streamwise vorticity by propagating to the right of the environmental vertical shear vector as shown in Fig. 1-2. Therefore, the existence of the mesocyclone in the supercell and its rightward deviating motion are dynamically linked to each other.

The cyclonically rotating supercell at its tornadic stage shows distinguishing characteristics near the surface as shown in Fig. 1-4. Gust fronts are generated between warm moist environmental winds and cold air outflows associated with forward flank downdraft (FFD) and rear flank downdraft (RFD). The one in the northeast is forward flank gust front (FFGF), and the other in the southwest is rear flank gust front (RFGF). An updraft (UD) is located around the intersection between the FFGF and RFGF. At this stage, a hook-shaped radar echo pattern becomes noticeable at the southeastern edge of the storm (thick line in Fig. 1-4), which indicates the existence of a strong cyclonic rotation at the altitude of about 1 km called a low-level mesocyclone. Rotunno and Klemm (1985) suggested that the source of the low-level mesocyclone is not only the

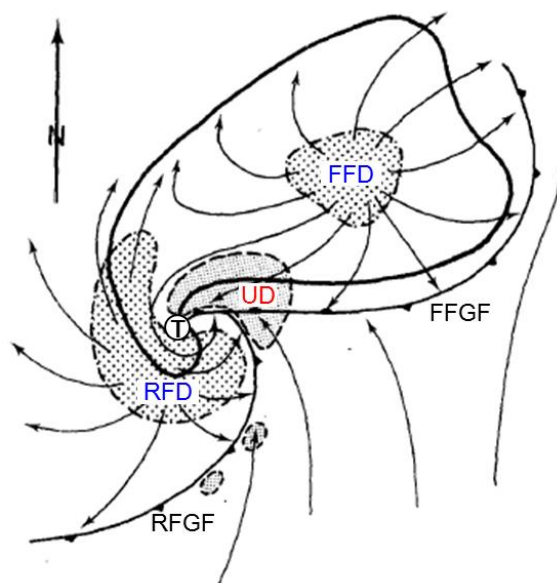


**Fig. 1-4.** Schematic plan view of a tornadic supercell at the surface. Thick line represents radar echo. Solid lines with frontal symbols represents gust fronts. The one in the northeast is forward flank gust front (FFGF), and the other in the southwest is rear flank gust front (RFGF). Arrows represent storm-relative winds. Positions of the updraft (UD), forward flank downdraft (FFD), and rear flank downdraft (RFD) are shown. The tornado location is denoted by the encircled T. (Adapted from Lemon and Doswell, 1979.)

environmental streamwise vorticity, but also a horizontal vorticity generated baroclinically along the FFGF.

On the other hand, the source of rotation of supercell tornado is still controversial. In their numerical study of Nobeoka, Miyazaki Prefecture tornado associated with Typhoon 0613, Mashiko et al. (2009) found that the source of the rotation of the tornado came from the horizontal vorticity of the environmental wind that has strong vertical shear near the surface. Schenkman et al. (2014) numerically studied two tornadoes spawned by a classical supercell in Oklahoma in the United States and suggested that frictionally generated horizontal vorticity near the surface is important for the source of rotation of the tornadoes. Mashiko (2016) numerically reproduced Tsukuba, Ibaraki Prefecture tornado (F3) and found that the source of the tornado was baroclinically generated horizontal vorticity. Furthermore, Noda and Niino (2010) made an idealized numerical simulation of a supercell tornado and suggested that the source of rotation of the tornado is the horizontal vorticity that is in the vertical shear of the environmental wind and is baroclinically generated due to horizontal density gradient. In any case, a tornadogenesis requires a source of rotation and a strong low-level updraft that causes horizontal convergence near the surface. The latter is considered to be caused by vertical gradient of the perturbation pressure due to low-level mesocyclone.

## **1.2. Environmental parameters for assessing tornado potential**

Since spatial and time scales of tornadoes are small, operational forecasts of tornado vortices using a direct numerical simulation is not practical. Instead, real-time tornado warnings based on the detection of a mesocyclone by Doppler radars or

potential forecast of tornado risk within a few days are issued. The latter is based on the forecast of mesocyclone-scale rotating updrafts by numerical models, and the forecast of several environmental parameters which assess the potential of supercells. Indeed, the tornado “nowcast” provided by Japan Meteorological Agency (JMA) is based on the potential risk of small-scale hazardous winds that are calculated by combining observed radar echoes, mesocyclone detection, and forecasted spatial distribution of the parameter called “the index related to small-scale hazardous winds” (Takishita, 2009; Fig. 1-5).

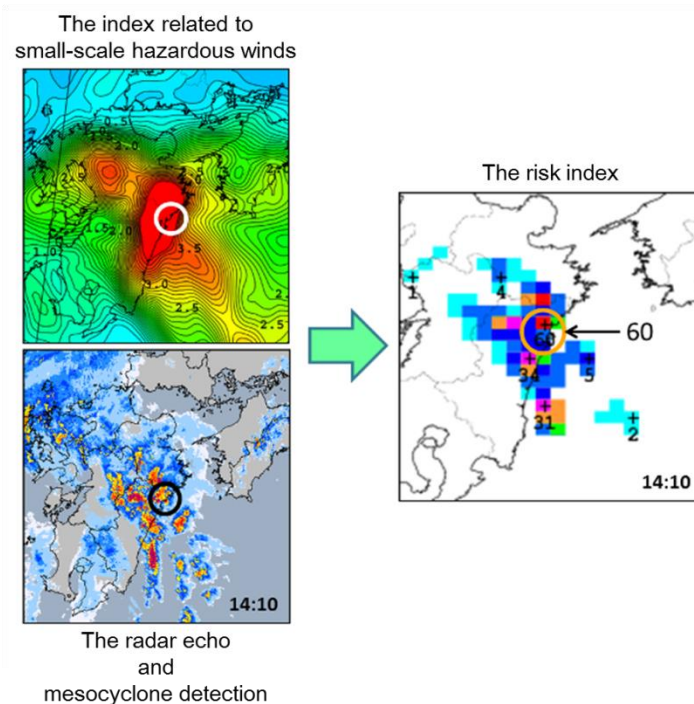


**Fig. 1-5.** A schematic image of the decision process for the risk index of small-scale hazardous winds adopted in JMA. (Adapted from the image open to the public in the JMA’s website: <http://www.jma.go.jp/jma/kishou/now/toppuu/tornado2-3.html>)

One of the most important parameters that give a potential for supercells (and possibly associated tornadoes) is storm-relative environmental helicity (SREH;

Davies-Jones et al., 1990). In general, SREH is calculated by integrating the product of horizontal wind speed and streamwise vorticity in the storm-relative reference frame ( $|\vec{V}_h - \vec{C}|$  and  $\omega_s$ , respectively; see Eq. (1.1) in section 1.1) from the surface to a given altitude  $H$ :

$$\text{SREH} = \int_0^H (\vec{V}_h - \vec{C}) \cdot \left( \vec{k} \times \frac{\partial \vec{V}_h}{\partial z} \right) dz, \quad (1.2)$$

SREH is a measure of the potential of environmental horizontal vorticity to produce mesocyclones through tilting, and is based on the understanding of the mechanism of supercell formation described in section 1.1. In a graphical view, SREH is proportional to the area enclosed by the tip of the storm motion vector  $\vec{C}$  and the wind hodograph between the surface and the altitude  $H$  (the red area in Fig. 1-6). By looking at the figure, we can easily understand that SREH becomes larger when the wind profile has a large vertical veering shear.

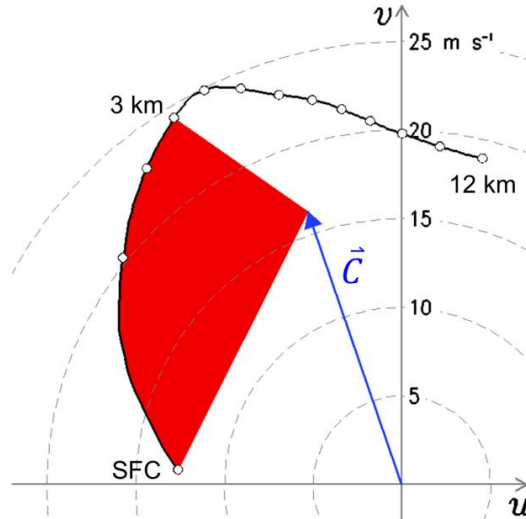


**Fig. 1-6.** An example of a hodograph (black solid line). Open circles on the hodograph are plotted at every 1-km height from the surface (SFC) to 12 km. If the storm motion vector  $\vec{C}$  is given by the blue arrow, SREH is proportional to the area enclosed by the tip of the vector  $\vec{C}$  and the hodograph between SFC and the altitude  $H$ . For example, SREH with  $H = 3$  km is equivalent to two times the red area in the  $u-v$  plane. The same hodograph will be shown later in Fig. 2-6a.

Another important parameter that gives a potential for supercells is convective available potential energy (CAPE). CAPE is defined as the vertical integration of positive buoyancy acting on an air parcel that is lifted from the near-surface height. The buoyancy  $B$  can be written as

$$B = -\frac{\rho_p - \bar{\rho}}{\bar{\rho}} g, \quad (1.3)$$

where  $\rho_p$  is the density of the parcel,  $\bar{\rho}$  is that of the environmental air, and  $g$  is the acceleration due to gravity. By using the equation of state and the approximation for the subsonic flow, we can obtain the following approximate expression for the moist atmosphere:

$$B \approx \frac{T_{vp} - \bar{T}_v}{\bar{T}_v} g, \quad (1.4)$$

where  $T_{vp}$  is the virtual temperature of the lifted parcel,  $\bar{T}_v$  is that of the environment. (Virtual temperature is defined as  $T_v \equiv T(1 + r_v/\varepsilon)/(1 + r_v)$ , where  $T$  is the temperature,  $r_v$  is the water vapor mixing ratio, and  $\varepsilon \equiv R_d/R_v$  is the ratio of the gas constant for dry air  $R_d$  to that for water vapor  $R_v$ .) CAPE is obtained by integrating the buoyancy from the level of free convection (LFC) to the equilibrium level (EL):

$$\text{CAPE} = \int_{\text{LFC}}^{\text{EL}} \frac{T_{vp} - \bar{T}_v}{\bar{T}_v} g \, dz. \quad (1.5)$$

(LFC is where  $T_{vp}$  starts to become larger than  $\bar{T}_v$ ; EL is where  $T_{vp}$  starts to become smaller than  $\bar{T}_v$ .) Since CAPE represents the maximum kinetic energy of upward motion that the lifted parcel obtains from the buoyancy, the potential maximum upward velocity of the moist convection is given by  $w_{\max} = \sqrt{2 \text{CAPE}}$ .

### **1.3. Tornadoes spawned by tropical cyclones**

Since the beginning of the 20th century, it has been known that tornadoes often occur in association with TCs (e.g., Gray, 1919; Mitchell, 1929). Hill et al. (1966) discussed that TCs' outer rainbands comprising long-lived discrete cells are favorable to tornado occurrences. Fujita et al. (1972) showed that the tornado associated with an outer rainband of Typhoon 7113 was spawned by a cyclonically rotating convective storm. McCaul (1987) showed that the tornado outbreak associated with Hurricane Danny in 1985 was spawned by a number of storms having a mesocyclone. He also noted that the environment for each storm had abundant streamwise horizontal vorticity and was favorable to the supercell development. Tornadoes spawned by TCs appear to be mainly caused by supercells. However, they are known to have some distinct characteristics that are different from those of classical supercells in the Great Plains of the United States.

Suzuki et al. (2000) analyzed tornado-spawning convective storms associated with Typhoon 9019 by using the Doppler radar installed at Meteorological Research Institute (MRI) in Japan. They found that these storms showed characteristics of "mini-supercells" whose horizontal and vertical scales were smaller than those of classical supercells that have long been subjects of the pioneering studies shown in section 1.1. The smaller size of TC-associated supercell is considered to be caused by relatively large near-ground vertical shear and modest CAPE for the TC environment. By using three-dimensional cloud model, McCaul and Weisman (1996) simulated a mini-supercell in a horizontally homogeneous basic state which was obtained by compositing TC-tornado environments. They concluded that strong dynamically induced pressure gradient forces caused by an interaction between the large near-ground

vertical shear and the updraft maintain the convection even if the buoyancy is moderate. Mashiko et al. (2009) succeeded in reproducing a tornado spawned by Typhoon 0613 at Miyazaki Prefecture by performing a quadruply nested numerical simulation. According to their analysis, the major source of vertical vorticity of the tornado was the storm-relative streamwise vorticity from the environment, in contrast to that spawned by a classical supercell where a substantial part of the source of tornado vortex is generated baroclinically along the edge of the cold pool.

If we look at the TC-scale, it is of interest to know that differences in the structure between TCs that spawn tornadoes and those that do not. Novlan and Gray (1974) showed that the vertical shear near the surface for tornadic hurricanes was larger than that for non-tornadic hurricanes. The vertical shear is now known to be one of the important ingredients for the supercell environment. Because of lack of available data and understanding of supercell storms at that time, however, they neither compared the three-dimensional structures of the TCs nor examined the distributions of environmental parameters such as SREH.

Previous studies have also revealed that tornado occurrences tend to be concentrated in the northeast quadrant of TCs (e.g., Hill et al., 1966; Orton, 1970; Novlan and Gray, 1974) or the right-front quadrant with respect to the moving direction of TCs (e.g., Smith, 1965; Fujita et al., 1972; McCaul, 1991, see Fig. 1-7a) in the Northern Hemisphere. McCaul (1991) found that the spatial distribution of tornadoes relative to the TC centers correlated strongly with that of the SREH (Fig. 1-7b), implying that the distribution of tornado occurrences is strongly related to the TC structure and its movement. However, McCaul (1991) did not investigate the SREH for non-tornadic TCs, so the differences between tornadic TCs and non-tornadic TCs have

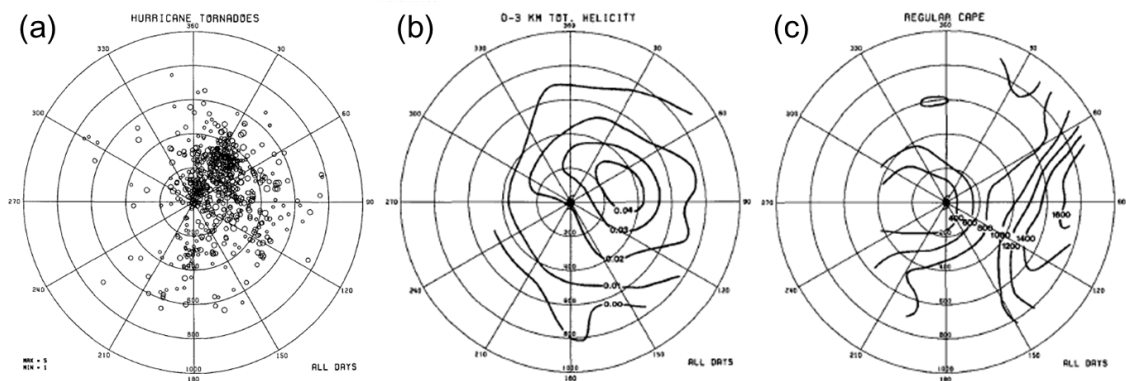


**Fig. 1-7.** (a) Locations of TC-spawned tornadoes in the United States (1948–86) with respect to the TC center and the moving direction of TC. (b) Composite horizontal distribution of SREH around the TCs. (c) Same as (b), but for CAPE. (From McCaul, 1991.)

not been clarified yet.

Furthermore, the relationship between thermodynamic instability and TC tornado occurrences remains uncertain. Novlan and Gray (1974) indicated that tornadic hurricanes had a slightly more stable lapse rate between 850 and 700 hPa than non-tornadic hurricanes. McCaul (1991) showed that the distribution of CAPE had almost no correlation with that of the tornadoes (Fig. 1-7c). While substantially large CAPE values of about  $2000 \text{ J kg}^{-1}$  were observed in some outbreaks of TC tornadoes (McCaul, 1987; Vescio et al., 1996), CAPE in a TC tornado environment is generally known to be fairly small: McCaul (1991) showed a mean value of  $253 \text{ J kg}^{-1}$ . Although the atmosphere must be conditionally unstable for tornadic convective storms to develop, parameters such as CAPE do not appear to be useful for assessing the risk of TC-spawned tornadoes.

#### **1.4. Purpose of this thesis**

TC-associated tornadoes are often spawned by mini-supercells, so the strong-shear environment seems to be necessary for their occurrences. However, the differences between tornadic TCs and non-tornadic TCs have not been clarified yet. On the other hand, previous studies suggest that the thermodynamic instability, which is considered to be important for the occurrences of supercells and associated tornadoes, does not seem to be important for occurrences of TC-associated tornadoes. The purpose of this thesis is therefore to clarify the distinctive factors for occurrences of the TC-spawned tornadoes from the viewpoint of the TC structure. For this purpose, the structure of tornado-spawning typhoons in Japan was investigated by means of a composite analysis, with an emphasis on environmental parameters that characterize the vertical shear and thermal instability. This thesis is organized as follows: Chapter 2 shows the results of the composite analysis. Chapter 3 shows the results of an idealized large eddy simulation of a mini-supercell which gives an estimate of entrainment rate used in the analysis in Chapter 2. General conclusions and future perspectives are given in Chapter 4.

## 2. Statistical Characteristics of Tornado-spawning Typhoons

### 2.1. Introduction

In this chapter, statistical characteristics of tornado-spawning typhoons are investigated. Main goal of this investigation is to clarify structural factors of typhoons which mainly contribute to the tornado occurrences. The analysis focuses on meso- $\alpha$  and larger scale properties ( $\geq O(100 \text{ km})$ ), because one of the interesting subjects related to tornadoes is whether such large scale conditions really affect the tornadogenesis on the order of 100–1000 m. Since the supercell on the order of 10 km is considered as a linker between the large-scale environment and the tornadogenesis, the environmental parameters explained in section 1.2 may give us some useful information. To achieve our goal, authentic tornado reports and reanalysis data of the atmosphere are needed.

In the present analysis, typhoons which approached Japan are divided into two groups on the basis of data provided by JMA: those that spawned tornadoes and those that did not. We may consider that differences between them are main contributors to the tornado occurrences. We will examine the structures of typhoons based on the environmental parameters of SREH and CAPE. Then, the results of the analysis based on the environmental parameters will be interpreted by examining three-dimensional distributions of horizontal wind, temperature, and humidity. This chapter is organized as follows: Section 2.2 describes the data and methods used for our analysis. Results of the SREH analysis are shown in section 2.3. Those of the CAPE analysis are shown in section 2.4. Section 2.5 discusses the results. Finally, summary and conclusions are given in section 2.6.

## **2.2. Data and methods**

### **2.2.1. Data sources and targets of analysis**

The times and locations of tornadoes that occurred in Japan were taken from “the Database of Small-scale Hazardous Winds Including Tornadoes” (<http://www.data.jma.go.jp/obd/stats/data/bosai/tornado/index.html>) provided by JMA. The typhoon-spawned tornadoes discussed in this paper are tornadoes including waterspouts near the seashore that occurred on the four large islands of Japan (Kyushu, Shikoku, Honshu, and Hokkaido Islands), within 550 km from the typhoon center. The distance between the typhoon center and the tornado was estimated from the JMA best track data. Fifty-three typhoon-spawned tornadoes, including two waterspouts, occurred during the analysis period between 1991 and 2013 (Fig. 2-1a); none occurred on Hokkaido Island located at the northern end. The tornado locations relative to the typhoon centers were concentrated in the northeast quadrant of the typhoon (Fig. 2-1b), which is consistent with previous studies on TC-spawning tornadoes (e.g., Hill et al., 1966; Orton, 1970; Novlan and Gray, 1974).

Typhoons accompanied by the typhoon-spawned tornadoes are defined as “tornadic typhoons” (TTs). To clarify the characteristics of TTs, it is necessary to adequately define “non-tornadic typhoons” (NTs) for comparison. In the present study, NTs are defined as typhoons which were at similar locations as TTs but did not spawn any tornadoes throughout their lifetimes. Practically, typhoons passing through areas within 100 km from the centers of TTs but not beyond 550 km from the corresponding tornado locations were selected as NTs.

To study the structures of TTs and NTs, we used the Japanese 55-year Reanalysis (JRA-55), which gives 6-hourly three-dimensional data having a horizontal resolution

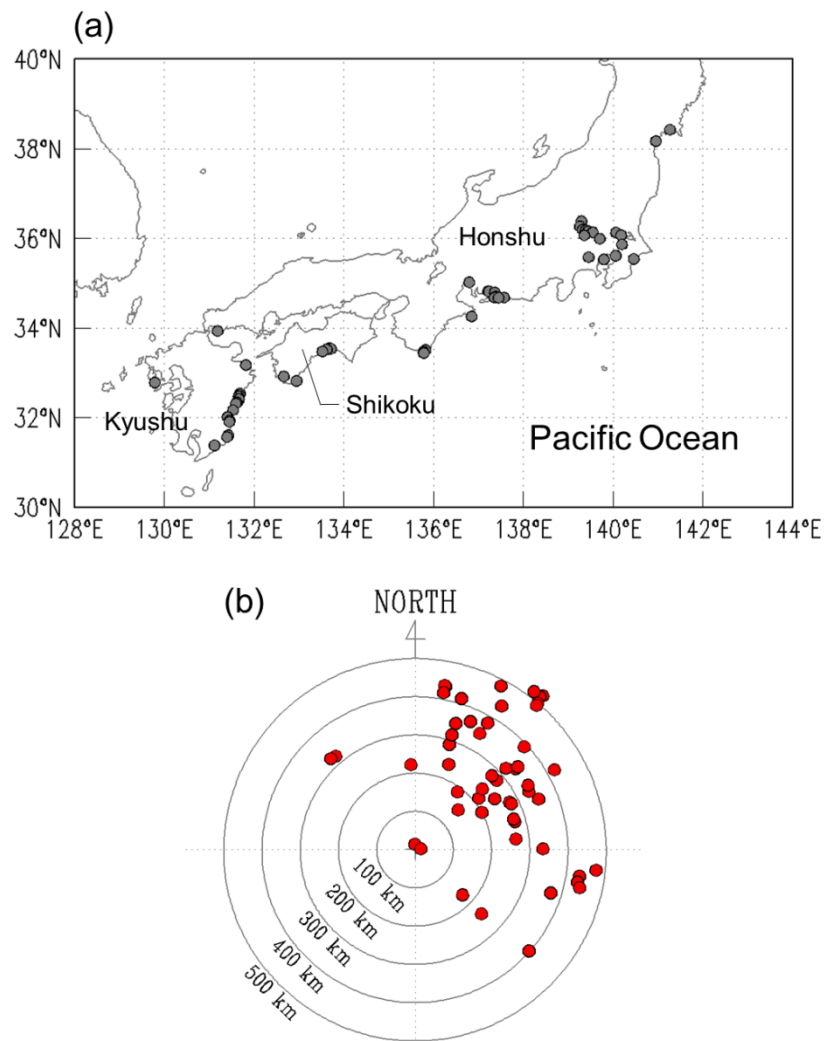


**Fig. 2-1.** (a) Geographical distribution of 53 typhoon-spawned tornadoes and (b) their distribution relative to the typhoon centers.

of 1.25° and 37 pressure levels from 1000 to 1 hPa (Kobayashi et al., 2015). In JRA-55, by wind profile retrievals surrounding the TCs (TCR; Fiorino, 2002), artificial profiles based on TCs' positions, maximum wind speeds, radii of 30 kt winds, and motions from best track data are assimilated near the TC centers besides the observational data. Since the intensity and size of a TC may affect the SREH and CAPE distributions in its vicinity, consideration of such information in the reanalysis data would enhance the validity of the present analysis. The structures of 34 TTs at the nearest 6-hourly time to

tornado occurrences are compared with those of 276 NTs. Note that the number of TTs is smaller than that of the typhoon-spawned tornadoes because several TTs spawned more than two tornadoes. Geographical locations of TTs and NTs are shown in Figs. 2-2 and 2-3, respectively.

### **2.2.2. Method of composite analysis**

In the present study, composite horizontal distributions of the environmental parameters around the typhoon centers both for TTs and NTs will be shown at first. Procedures of the composite are as follows:

- The reference coordinate system is taken in the way that the center of each typhoon and the north direction coincide with the origin and the y axis, respectively.
- Physical quantities such as geopotential height, horizontal wind, temperature, and relative humidity at each pressure level in JRA-55, which are required for the parameter calculation, are interpolated to equally-spaced horizontal grid points in the reference coordinate system by applying the cubic convolution interpolation method (Key, 1981).
- Environmental parameters around each typhoon center are calculated from the vertical profiles of the interpolated physical variables at the horizontal grid points in the reference coordinate system.
- Composite distributions of the environmental parameters are obtained by simply superposing the typhoon centers and averaging them for TTs and NTs, respectively.

In each analysis, the statistical significance of the difference between TTs and NTs is evaluated by Welch's *t* test.

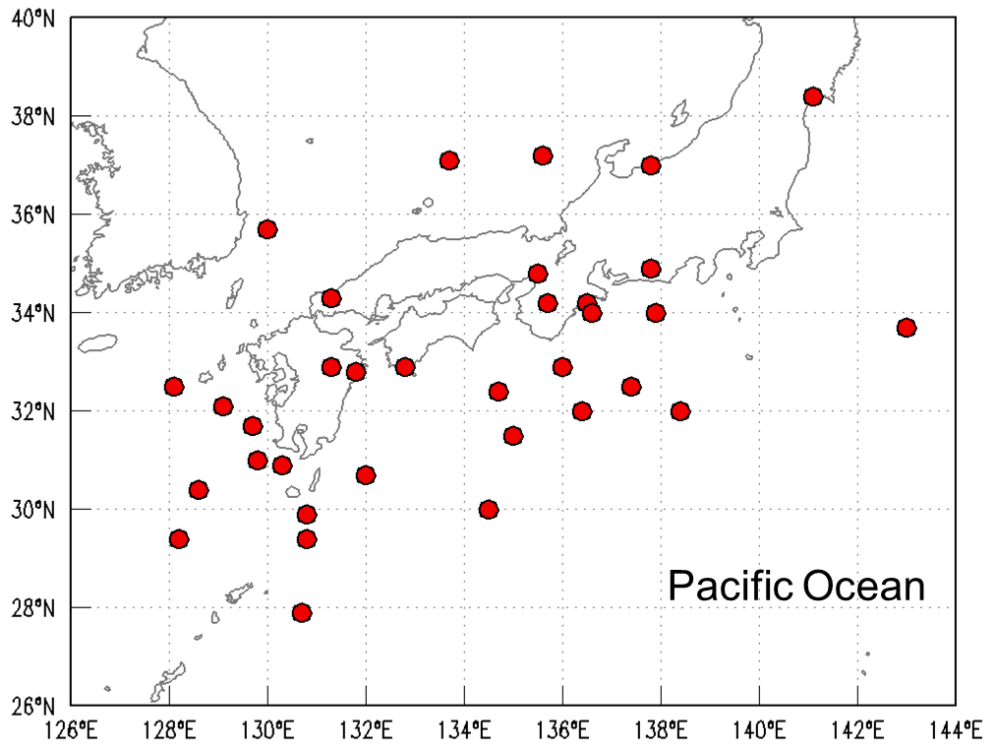


**Fig. 2-2.** Geographical distribution of 34 TTs.

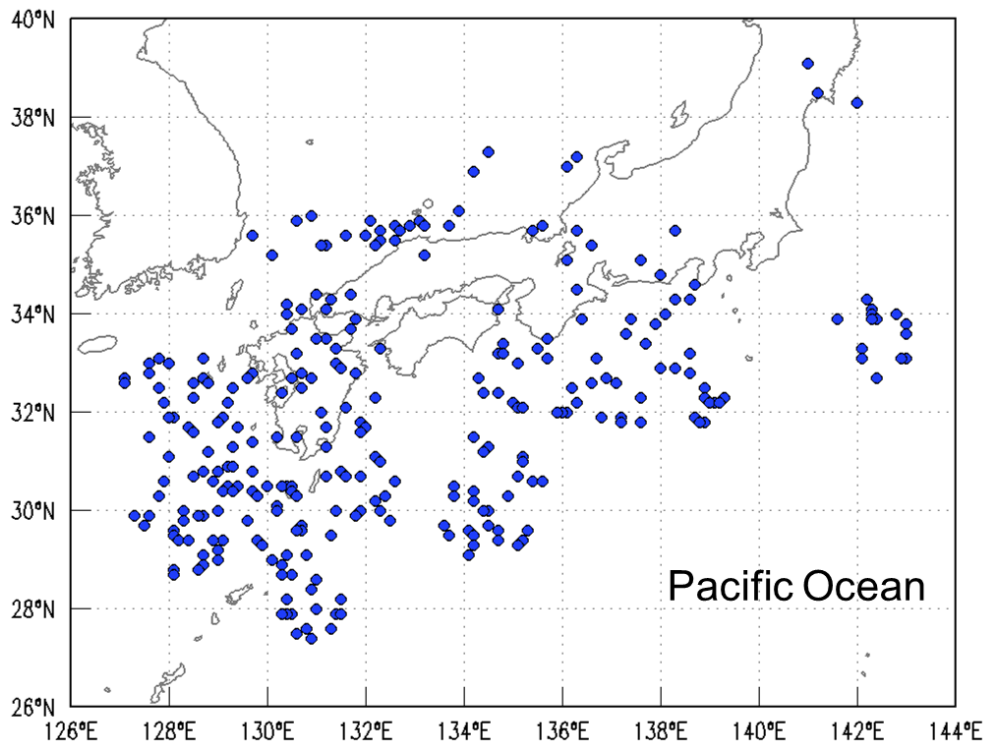


**Fig. 2-3.** Geographical distribution of 276 NTs.

### **2.2.3. Method of time series analysis**

While the composite analysis will simply show the difference in the value of the parameter between TTs and NTs, and show the relationship between the spatial distribution of the parameter and that of tornado occurrences, it is not sufficient to elucidate the direct correspondence between each tornado occurrence and temporal change in the parameter values. In order to examine this correspondence, a time series analysis was made. The time series of the parameters are prepared in the following manner:

- The origin of the time axis ( $t = 0$  h) is taken as the time of each tornado occurrence.
- The grid point values of the physical quantities of JRA-55 are interpolated to locations of the tornadoes every hour by applying the cubic convolution interpolation method with respect to latitude, longitude, and time.
- The hourly parameter values at the location of the tornado occurrence are calculated from the interpolated profiles.

The statistical significance of the difference between the value at  $t = 0$  h and that at other time is evaluated by Welch's  $t$  test.

## **2.3. Analysis of SREH**

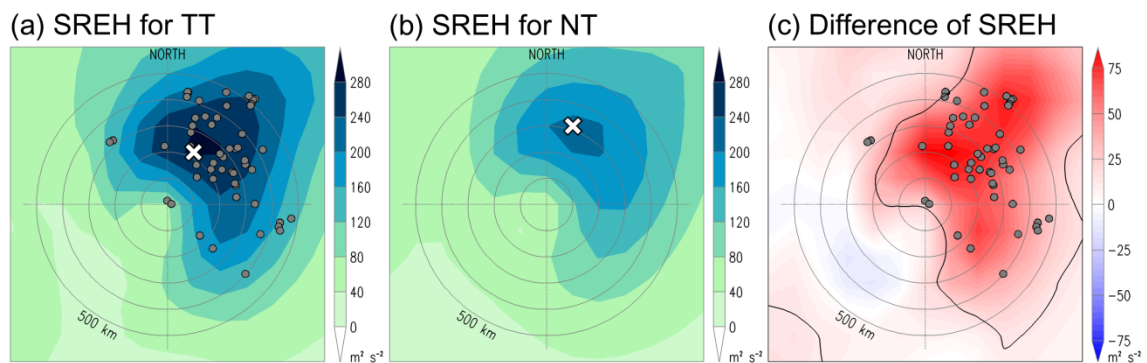
### **2.3.1. Calculation of SREH**

SREH was calculated on the basis of geopotential height and horizontal wind at pressure levels in JRA-55. JRA-55 has a relatively high vertical resolution at the low levels, which enables relatively accurate calculation of SREH. (The integration for  $H = 3$  km was calculated by using its 10–12 levels within 1000, 975, 950, 925, 900, 875, 850, 825, 800, 775, 750, and 700 hPa.) Since there is no information about the movement of

each convective storm, the storm motion vector ( $\vec{C}$  in Eq. (1.2)) needs to be estimated from the quantities that characterize the storm environment. In the present study,  $\vec{C}$  was calculated from the vertical profile of horizontal wind by using the method of Bunkers et al. (2000).

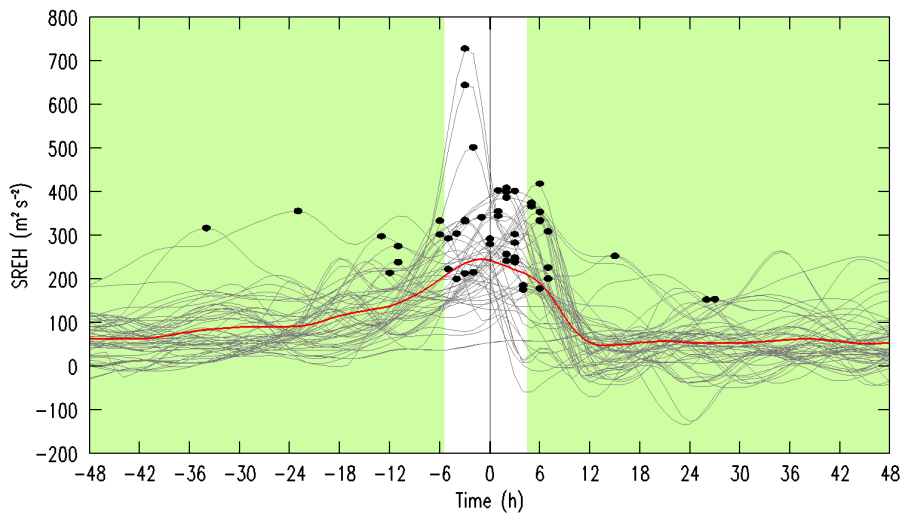
### 2.3.2. Composite distribution and time series

Fig. 2-4 shows composite horizontal distributions of SREH with  $H = 3$  km around the typhoon center for TT and NT. SREH is large in the northeast (NE) quadrant both for TT and NT (Figs. 2-4a, b, respectively), and its distribution is consistent with that of the tornado locations. Note that SREH with  $H = 3$  km gives the highest correlation with the tornado distribution (not shown). The SREH for TT is much larger than that for NT, particularly in the eastern semicircle (Fig. 2-4c). The composite shows that SREH is a useful parameter that can account for the distribution of tornado occurrences and can distinguish TTs from NTs.



**Fig. 2-4.** Composite horizontal distribution of SREH with  $H = 3$  km around the typhoons: (a) for TT and (b) for NT. (c) the difference in the values of TT from those of NT. Locations of maximum values within the displayed area are shown by the cross marks in (a) and (b). The areas in which the difference between TTs and NTs are statistically significant at 5% based on Welch's  $t$  test are enclosed by solid black lines in (c). Solid gray circles in (a) and (c) show locations of tornadoes relative to the typhoon centers.

Fig. 2-5 shows the time series of SREH for all typhoon-spawning tornadoes. The maxima of SREH, shown in the figure by black circles, are clearly concentrated around the time of tornadoes. The averaged SREH (red line in Fig. 2-5) increases gradually until a few hours before the tornado occurrences, reaches its maximum of  $247 \text{ m}^2 \text{ s}^{-2}$  slightly before the time of tornadoes, and finally decreases to about  $50 \text{ m}^2 \text{ s}^{-2}$ . This demonstrates that SREH can adequately assess the risk of tornado occurrences associated with the typhoon approaches.



**Fig. 2-5.** Temporal variations of SREH at the locations of 53 tornadoes (gray lines). The origin of the time axis ( $t = 0 \text{ h}$ ) is taken as the time of each tornado occurrence. A black circle shows the maximum value for each tornado event. The red line represents a temporal variation in the mean values for the 53 tornadoes. The light green shading indicates the time when the parameter values are smaller than those at the time of tornadoes with a statistical significance of 5% based on Welch's  $t$  test.

### 2.3.3. Factors contributing to larger SREH of TTs

本項については、5年以内に雑誌等で刊行予定のため、非公開。

### 2.3.4. Interpretation by cyclone phase space

本項については、5年以内に雑誌等で刊行予定のため、非公開。

## 2.4. Analysis of CAPE

### 2.4.1. Calculation of CAPE

CAPE was calculated on the basis of geopotential height, temperature, and relative humidity at pressure levels in JRA-55. The lifted parcel is assumed to have initial potential temperature and mixing ratio, which are given as their averages over the lowest 1-km layer, respectively, where the lowest 1-km layer average was obtained by using 4–5 levels within 1000, 975, 950, 925, 900, and 875 hPa.

As reviewed in section 1.3, the relationship between thermodynamic instability and tornado occurrences associated with typhoons are unclear. Recently, Molinari et al. (2012) suggested that entraining CAPE (E-CAPE) including the effects of entrainment of environmental air can adequately represent the asymmetric distribution of convective activities around TCs. Therefore, two kinds of CAPEs are examined in the present study: one is “ordinary CAPE” (hereafter, referred to simply as CAPE), for which the equivalent potential temperature of the lifted parcel is conserved. The other is E-CAPE, for which the temperature and mixing ratio of the parcel are calculated by considering the effects of entrainment on the basis of the Lagrangian parcel model (Romps and Kuang, 2010). In the calculation of E-CAPE,  $T_{vp}$  in Eq. (1.5) changes depending on the thermodynamic profile above the boundary layer. All of the condensates were assumed to fall immediately from the parcel. Latent heat release associated with freezing was not considered. We also followed Molinari et al. (2012) to assume that the parcel ascends at a speed of  $1 \text{ m s}^{-1}$  and entrains environmental air at a constant mass entrainment rate  $\epsilon$ . This study demonstrates that a suitably defined E-CAPE can be a useful parameter for assessing the potential of tornado occurrences associated with typhoons for the first time.

### 2.4.2. Composite distribution and time series

Fig. 2-6 shows the composite horizontal distributions of CAPE and E-CAPE. CAPE is large in the southeastern (SE) side of both TT (Fig. 2-6a) and NT (Fig. 2-6b). This result is consistent with the composite distribution of CAPE based on rawinsonde observations around the tornado-spawning TCs with respect to their moving directions (McCaul, 1991; see Fig. 1-7c) if we note that TTs in our study generally headed north-northeast. As noted in McCaul (1991), the distribution of CAPE is not consistent with that of the tornado locations. The difference in CAPE for TT from that for NT (Fig. 2-6c) shows that the CAPE for TT in the NE quadrant, where tornadoes are concentrated, is not larger than that for NT. Furthermore, the CAPE in the northwest side for TT is smaller than that for NT with a statistical significance of 5% based on Welch's  $t$  test. These results imply that CAPE is not a suitable parameter for assessing

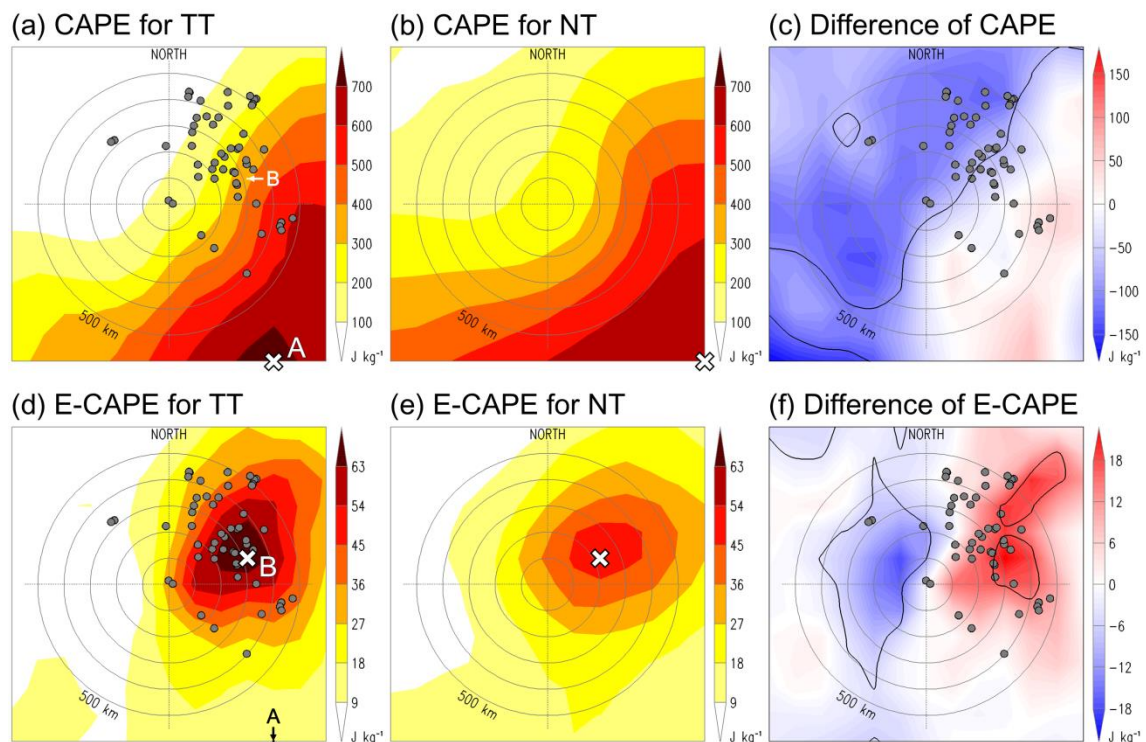


Fig. 2-6. Same as Fig. 2-4, but for (a)–(c) CAPE and (d)–(f) E-CAPE.

the potential of tornado occurrences in typhoons.

In contrast, E-CAPE with  $\epsilon = 20\% \text{ km}^{-1}$  is large in the NE quadrant for both TT and NT (Figs. 2-23d, e, respectively), and its distribution for TT is consistent with that of the tornado locations. Note that the values of E-CAPE are about an order of magnitude smaller than those of CAPE. E-CAPE in the NE quadrant of TT tends to be larger than that of NT, where the difference is statistically significant in some regions of the quadrant (Fig. 2-6f). Thus, E-CAPE better accounts for the distribution of tornado occurrences and distinguishes TTs from NTs than CAPE does.

Fig. 2-7 shows time series of CAPE and E-CAPE. CAPE values are often large well before the time of tornadoes; an increase in CAPE does not necessarily correspond to tornado occurrence (Fig. 2-7a). CAPE averaged for all cases (red line in Fig. 2-7a) shows a decreasing trend from  $-48$  to  $-15$  h, weakly increases until  $0$  h, and eventually approaches zero. Welch's  $t$  test shows that CAPE after  $8$  h is smaller than its value at  $0$  h with statistical significance of  $5\%$  (light green shading in Fig. 2-7a), but that before  $0$  h does not give useful information. On the other hand, E-CAPE before  $0$  h tends to be smaller than that near the time of tornadoes (Fig. 2-7b). The averaged E-CAPE (red line in Fig. 2-7b) remains nearly constant from  $-48$  to  $-15$  h, increases toward its maximum slightly before  $0$  h, and finally approaches zero. E-CAPE except from  $-4$  to  $2$  h is smaller than its value at  $0$  h with a statistical significance of  $5\%$ . Thus, an increase of E-CAPE has a clear relation to the tornado occurrences.

### **2.4.3. Impacts of entrainment on the distribution of CAPE**

It is of interest to know why the distribution of CAPE changed dramatically by including the effects of entrainment as shown in Figs. 2-23 and 2-24. Fig. 2-8 shows

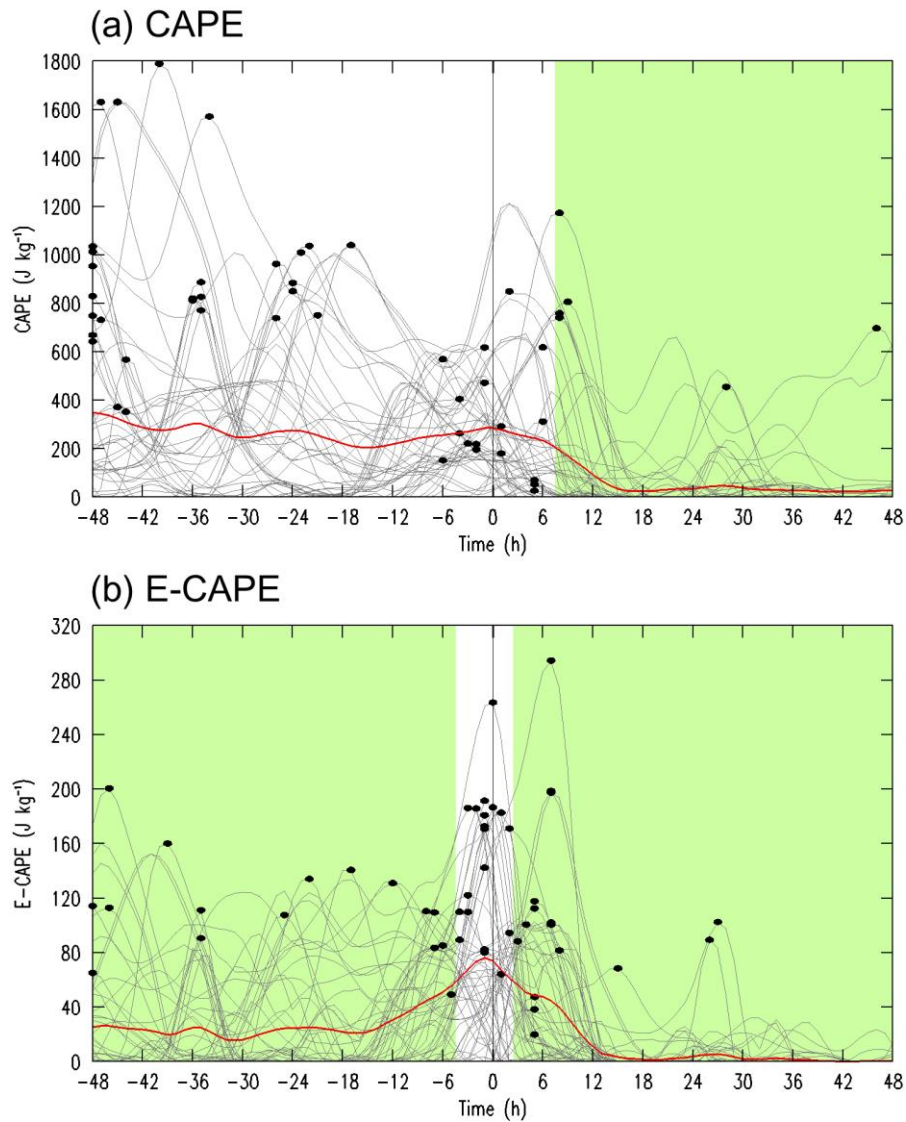


**Fig. 2-7.** Same as Fig. 2-5, but for (a) CAPE and (b) E-CAPE.

the composite profiles of potential temperature  $\theta$ , relative humidity (RH), and equivalent potential temperature  $\theta_e$  for TT at the point of the maximum composite CAPE in the SE side (the cross mark in Fig. 2-6a: hereafter, referred to as Point A) and those at the point of the maximum composite E-CAPE in the NE quadrant (the cross mark in Fig. 2-6d: hereafter, Point B). Also shown in Fig. 2-8c are the variations of  $\theta_e$  for lifted parcels with and without entrainment.

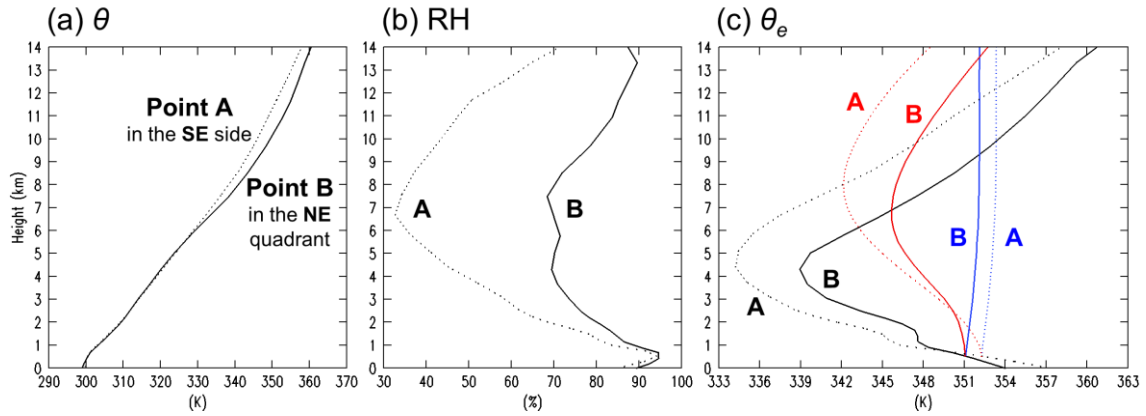


**Fig. 2-8.** Composite vertical profiles of (a) potential temperature  $\theta$ , (b) relative humidity (RH), and (c) equivalent potential temperature  $\theta_e$  for TT. Also shown in (c) are variations of  $\theta_e$  for lifted parcels. Dotted lines show the profiles at Point A in Fig. 2-6a and solid lines show those at Point B in Fig. 2-6d. In (c), black lines show the environmental profiles, blue lines show variations in the lifted parcels without entrainment, and red lines show those with entrainment.

Without entrainment, the parcel conserves  $\theta_e$  during its ascent (blue lines in Fig. 2-8c); thus CAPE is determined solely by the initial  $\theta_e$  of the parcel and the environmental virtual temperature lapse rate. At Point B in the NE quadrant, the initial  $\theta_e$  is lower (Fig. 2-8c) because the near-surface  $\theta_e$  around the typhoon becomes lower toward the north as shown in Fig. 2-9a. Furthermore, the stratification above an altitude of 6 km is more stable (Fig. 2-8a) because Point B is located closer to the warm core near the center than Point A (Fig. 2-9b). Therefore, CAPE at Point B is smaller than that at Point A. If the effects of entrainment are considered, however,  $\theta_e$  of the parcel is affected by the environmental  $\theta_e$  to approach the latter (red lines in Fig. 2-8c), so the distribution of the mid-tropospheric moisture shown in Fig. 2-9c becomes an important contributor to that of E-CAPE. At point A, the environmental  $\theta_e$  at an altitude of about 4.5 km is relatively low (black dotted line in Fig. 2-8c) owing to the dry mid-troposphere (dotted line in Fig. 2-8b). Thus,  $\theta_e$  of the parcel decreases significantly as it ascends, and the total buoyancy obtained by the parcel is reduced.

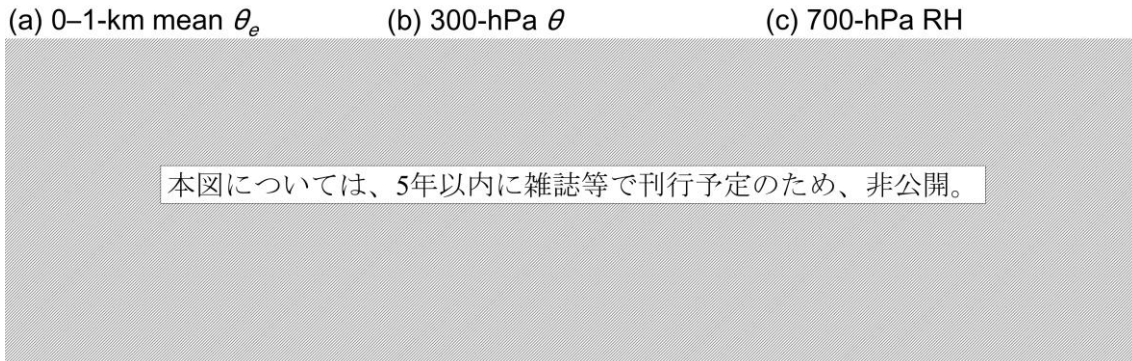


**Fig. 2-9.** Composite horizontal distributions of (a) 0–1-km mean  $\theta_e$ , (b) 300-hPa  $\theta$ , and (c) 700-hPa RH for TTs. Solid gray circles show the locations of tornadoes relative to the typhoon centers. Labels A and B correspond to those in Fig. 2-6.

At Point B, however, such a reduction in the environmental  $\theta_e$  is moderate (black solid line in Fig. 2-8c) because of the moist mid-troposphere (solid line in Fig. 2-8b). Thus, the reduction of  $\theta_e$  of the parcel is less than that at Point A (red solid line in Fig. 2-8c). Furthermore, the stratification above an altitude of 6 km becomes less important for E-CAPE because the effects of entrainment lower the equilibrium level. For these reasons, E-CAPE in the NE quadrant becomes larger than that in the SE side.

#### 2.4.4. Main factor contributing to larger E-CAPE of TTs

E-CAPE generally becomes relatively large in the NE quadrant because of the moist mid-troposphere, which is common in both TTs and NTs. After a detailed inspection of the temperature and water vapor distributions, a larger E-CAPE for TTs is considered to be caused by a larger temperature lapse rate, especially between 850 and 550 hPa ( $\Gamma_{850-550}$ ), in the NE quadrant (Fig. 2-10). In fact, if the temperature profiles between 850 and 550 hPa for TTs are artificially modified in a way that the composite  $\Gamma_{850-550}$  for TT (Fig. 2-10a) becomes the same as that for NT (Fig. 2-10b), the difference in E-CAPE between TT and NT almost vanishes in the region where tornadoes are

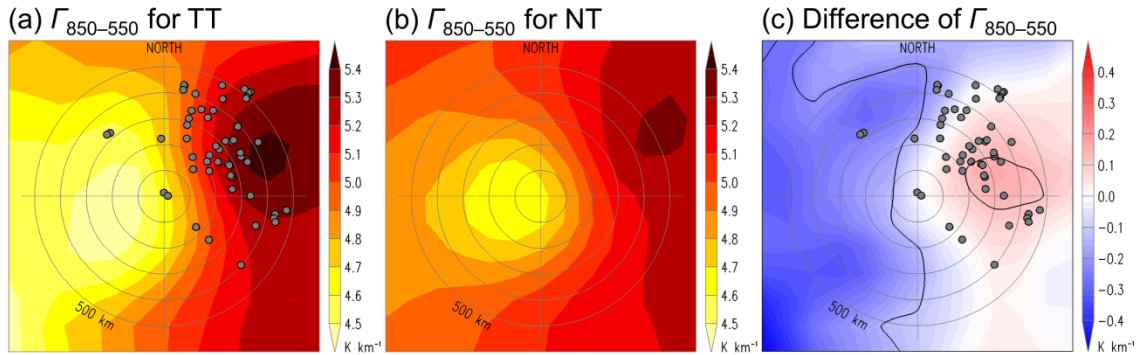


**Fig. 2-10.** Composite horizontal distribution of the temperature lapse rate between 850 and 550 hPa ( $\Gamma_{850-550}$ ): (a) for TT and (b) for NT. (c) the difference of  $\Gamma_{850-550}$  for TT from that for NT. Solid gray circles in (a) and (c), and solid black lines in (c) are same as those in Fig. 2-4.

concentrated. While  $\Gamma_{850-550}$  is large to the north-northeast of the typhoon centers for both TT and NT, its maximum for TT is larger than that for NT and is located closer to the typhoon center. The point where the composite  $\Gamma_{850-550}$  for TT minus that for NT is the largest (Fig. 2-10c) coincides with the point where the composite E-CAPE for TT is maximum (the cross mark in Fig. 2-6d). At that point, the averaged  $\Gamma_{850-550}$  for TTs is  $0.17 \text{ K km}^{-1}$  larger than that for NTs, which is equivalent to 31% of the averaged E-CAPE for TTs.

$\Gamma_{850-550}$  plays an important role in E-CAPE because the loss of buoyancy of the lifted parcel through entrainment lowers the equilibrium level to about 550 hPa. Without entrainment, the equilibrium level is much higher, so that ordinary CAPE is less sensitive to the conditionally unstable layer up to 550 hPa, which is different between TTs and NTs. One of the possible mechanisms causing the larger temperature lapse rates of the layer for TTs may be a dry intrusion into the NE quadrant (e.g., Hill et al., 1966; McCaul, 1987) and associated cooling due to the evaporation of raindrops at about 550 hPa. Curtis (2004) showed that most tornado outbreaks associated with the land-falling TCs occurred below dry intrusions at midlevel. However, the cause of the larger lapse rates

requires further investigation in future.

#### 2.4.5. Sensitivity to entrainment rate

In this subsection, sensitivity of the E-CAPE distribution to the entrainment rate is examined. Figs. 2-28 and 2-29 show the composite horizontal distributions and the time series of E-CAPE for  $\epsilon = 10\% \text{ km}^{-1}$ , half of the value used in the main analysis, respectively. Compared with the composite for  $20\% \text{ km}^{-1}$  (Figs. 2-23d, e), the maximum points of E-CAPE are located farther from the typhoon centers both for TTs

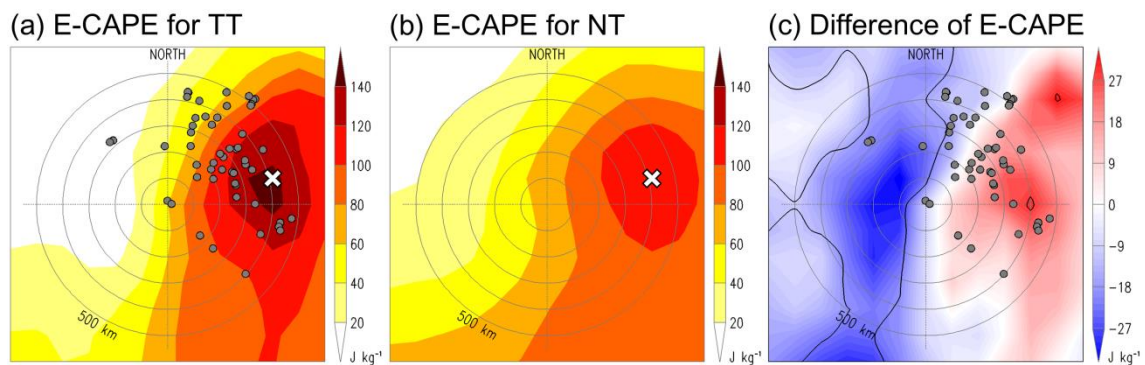


Fig. 2-11. Same as Fig. 2-4, but for E-CAPE with  $\epsilon = 10\% \text{ km}^{-1}$ .

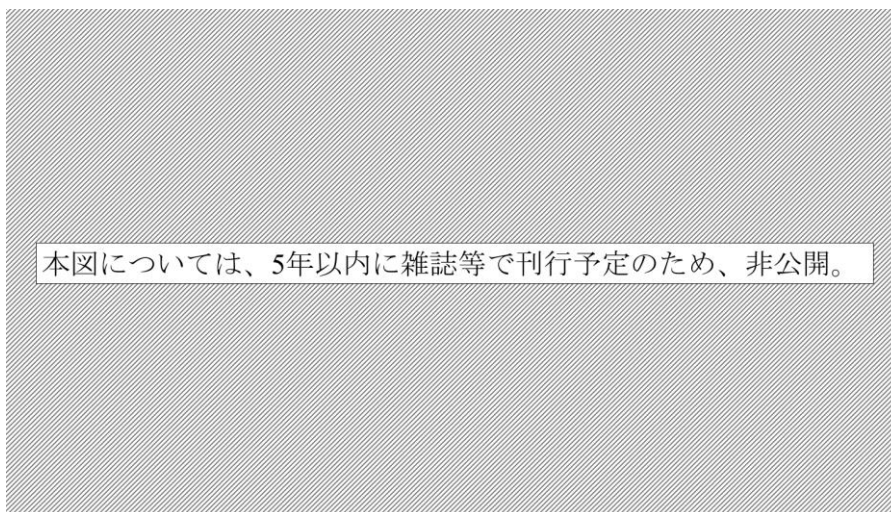
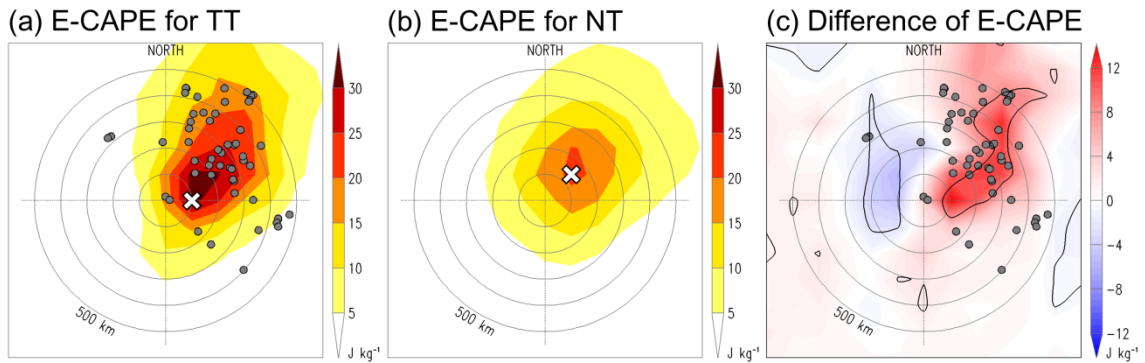


Fig. 2-12. Same as Fig. 2-5, but for E-CAPE with  $\epsilon = 10\% \text{ km}^{-1}$ .

and NTs (Figs. 2-28a, b), so the distribution for TT is less consistent with the distribution of tornado occurrences. Furthermore, the difference between TTs and NTs is less significant than that for 20%  $\text{km}^{-1}$  (Fig. 2-11c). The time series shows that the rises in E-CAPE with  $\epsilon = 10\% \text{ km}^{-1}$  around 0 h tend to be more moderate than those for 20%  $\text{km}^{-1}$ , so that the time period outside of which the E-CAPE is smaller than that at the tornado occurrence becomes wider (Fig. 2-12).

When  $\epsilon$  is doubled to 40%  $\text{km}^{-1}$ , on the other hand, the maximum points of E-CAPE tend to be located closer to the typhoon center for both TTs and NTs (Figs. 2-30a, b). As a result, they are located at the smaller radius than the region where tornadoes are concentrated for TT. Larger  $\epsilon$  promotes higher contribution of mid-tropospheric moisture to E-CAPE, so that E-CAPE tends to have relatively large values in regions where the atmosphere is almost saturated. The time series shows that another peak appears after the time of tornadoes in addition to the main peak (Fig. 2-14). The former peak corresponds to another E-CAPE maximum close to the typhoon center. Such double peaks make it difficult to evaluate the risk of tornadoes associated with the typhoon approaches properly. Thus, E-CAPE with  $\epsilon = 40\% \text{ km}^{-1}$  appears to be less suitable than that for 20%  $\text{km}^{-1}$ , although the difference between TTs and NTs becomes more significant (Fig. 2-13c).

The sensitivity analysis shows that E-CAPE with  $\epsilon = 20\% \text{ km}^{-1}$  gives the best results for explaining the occurrences of the typhoon-spawning tornadoes. This entrainment rate is larger than that in Molinari et al. (2012), who noted that  $\epsilon$  in the range of 5–10%  $\text{km}^{-1}$  gave the best distribution of E-CAPE for explaining that of lightning activities around TCs. To apply E-CAPE to future operational forecasting of the tornado potential, it is important to verify whether the entrainment rate used in the



**Fig. 2-13.** Same as Fig. 2-4, but for E-CAPE with  $\epsilon = 40\% \text{ km}^{-1}$ .

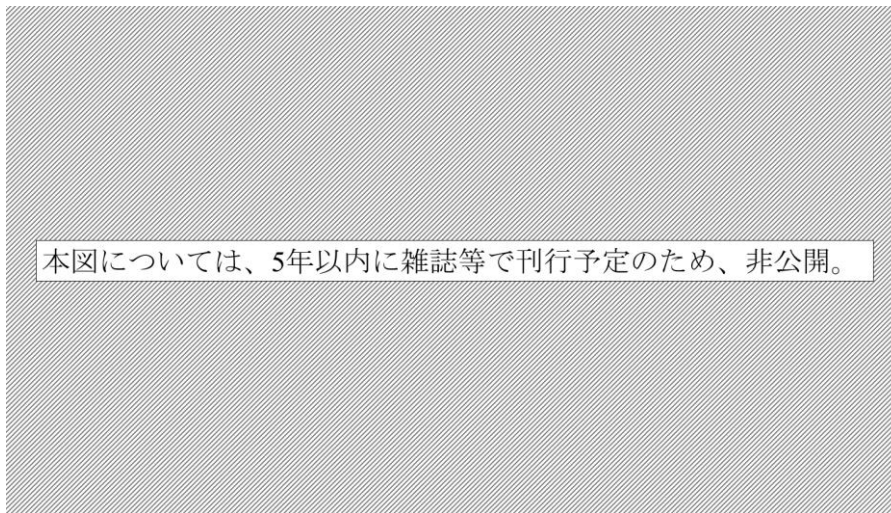


**Fig. 2-14.** Same as Fig. 2-5, but for E-CAPE with  $\epsilon = 40\% \text{ km}^{-1}$ .

E-CAPE calculation is physically reasonable. This is investigated in the next chapter.

## 2.5. Discussion

本節については、5年以内に雑誌等で刊行予定のため、非公開。

## 2.6. Summary and conclusions

Storm-relative environmental helicity (SREH) for tornadic typhoons (TTs) in the northeast quadrant, where the tornado occurrences are concentrated, is significantly larger than that for non-tornadic typhoons (NTs). This demonstrates that the structure of

TTs is favorable to the supercell generation. Larger SREH for TTs is mainly attributed to larger vertical veering shear in the northeast quadrant. Two factors contribute to the larger shear for TTs: one is stronger intensity of typhoon and the other is larger synoptic-scale vertical wind shear superposed on the typhoon vortex. The former contributes to near-ground vertical shear and the latter contributes to mid-level vertical shear. Furthermore, faster synoptic-scale wind speed at the mid-troposphere that increases the propagation speeds of supercells also contributes to the larger SREH for TTs.

Since the synoptic-scale wind properties are essentially important for the SREH around typhoons, the index of cyclone's symmetry,  $B$ , which is one of the parameters composing the cyclone phase space, can distinguish TTs from NTs:  $B$  for TTs is significantly larger than that for NTs. Considerable number of TTs satisfy the criterion for the onset of extratropical transition ( $B > 10$  m), indicating that TTs are affected by the mid-latitude baroclinic zone more strongly than NTs.

Convective available potential energy (CAPE) including the effects of entrainment (Entraining CAPE: E-CAPE) for TTs is also larger than that for NTs, which demonstrates that the thermodynamic structure of TTs is favorable to convection. Larger E-CAPE for TTs can be mainly attributed to larger temperature lapse rate in the mid-troposphere. On the other hand, ordinary CAPE, which does not consider the effects of entraining mid-tropospheric unsaturated air and overestimates total buoyancy obtained by a lifted air parcel, cannot distinguish TTs from NTs.

It is a new finding that E-CAPE rather than ordinary CAPE is a suitable parameter for assessing the thermodynamic instability which contributes to the tornado occurrences associated with typhoons. The results of the composite analysis and time

series analysis imply that the entrainment rate of about  $20\% \text{ km}^{-1}$  gives the most appropriate E-CAPE for assessing the potential of typhoon-spawned tornadoes. Since this estimate of the entrainment is based on indirect evidence, however, we need to examine the actual entrainment rate for supercells associated with typhoons.

### **3. Large Eddy Simulations for Estimating Entrainment Rates of Typhoon-associated Supercells**

本章については、5年以内に雑誌等で刊行予定のため、非公開。

## 4. General Conclusions and Future Perspectives

Structure of tornado-spawning typhoons is characterized by large storm-relative environmental helicity (SREH) and large entraining convective available potential energy (E-CAPE) in their northeast quadrants, which result in high potential for generating cyclonically-rotating supercells.

Large SREH is mainly caused by three factors: the first is typhoon intensity which contributes to strength of vertical wind shear near the ground. Typhoon intensities for tornadic typhoons (TTs) are usually stronger than those for non-tornadic typhoon (NTs), which results in larger near-surface SREH for TTs. The second is the synoptic-scale vertical wind shear superposed on the typhoon vortex, which contributes to strength of vertical shear in the mid-level. Above the altitude of 1 km, the synoptic-scale vertical shear for TTs is larger than that for NTs, which results in the larger mid-level SREH for TTs. These two factors are combined to generate larger vertical veering shear for TTs. The third is the mid-level synoptic-scale wind speed which determines the propagation speed of supercells. Since the mid-level synoptic-scale flows for TTs tend to be stronger than those for NTs, the storm propagation speed for TTs becomes faster, so that the near-surface SREH for TTs increases more.

The parameter representing cyclone's symmetry,  $B$ , which is one of the three parameters of the cyclone phase space, also exhibit notable characteristics of tornado-spawning typhoons.  $B$  is related to the synoptic-scale baroclinicity, and larger  $B$  is likely to be caused by larger synoptic-scale vertical wind shear and possibly larger synoptic-scale wind speed in the mid-troposphere. The mean value of  $B$  for TTs is significantly larger than that for NTs and majority of TTs satisfy the criterion for the

onset of extratropical transition ( $B > 10$  m). Extratropical transition seems to be the key for tornado occurrences associated with typhoons.

Effectiveness of E-CAPE for assessing the risk of typhoon-spawned tornadoes is first demonstrated in the present study. In contrast to ordinary CAPE without the entrainment effects, E-CAPE gives a consistent distribution with the locations of tornado occurrences and can distinguish TTs from NTs. Larger E-CAPE for TTs can be mainly attributed to larger temperature lapse rate in the mid-troposphere. This thermodynamic instability, which is distinctive of TTs, cannot be detected by ordinary CAPE because it cannot consider the effects of entraining mid-tropospheric unsaturated air, and thus overestimates total buoyancy obtained by the lifted parcel. It is important to explicitly consider the entrainment effects in accurate evaluation of the risk of typhoon-associated supercells.

E-CAPE with a constant entrainment rate of  $20\% \text{ km}^{-1}$  appears to give the most consistent spatial distribution around the typhoon and temporal variation at the location of tornado. An idealized numerical experiment of supercell in typhoon environment performed by large eddy simulation (LES) gave a physical evidence of the value of entrainment rate. A simple one-dimensional entraining plume model gives a reasonable approximation of an updraft plume of the simulated supercell in the layer from the top of the boundary layer to the mid-troposphere. In this layer, estimated entrainment rates shows about  $15\text{--}20\% \text{ km}^{-1}$ , which is consistent with the assumption of the above E-CAPE calculation. Since the simulated supercell shows typical characteristics of typhoon-associated supercells, the result can be considered as a representative of those supercells.

In this thesis, structural factors of typhoons which mainly contribute to tornado

occurrences are revealed. The present study, however, considered only typhoons which approached Japan surrounded by the sea. It is of interest to examine tornado-spawning hurricanes in the United State where tornadoes develop over land which has larger friction and experiences larger surface heating than over ocean. For further understanding of the environment of TC-associated tornadoes, we need to clarify its similarities and differences between Japan and the United States.

Effectiveness of E-CAPE for assessing the potential of typhoon-spawned tornadoes is clarified in the present study. This motivates us to examine whether E-CAPE is also a useful index for tornadoes which occur in different environments, and other types of severe weather events like downbursts, hail, flash floods, and so on. It is necessary to conduct further research subject to those events by using the similar approach to the present analysis.

In the present study, a constant entrainment rate is assumed in the E-CAPE calculation. However, the results of LES show that actual entrainment rates change with height. If we can parameterize entrainment rates quantitatively by environmental quantities such as vertical wind shear and condition of stratification or properties of storm itself such as updraft intensity and storm-relative wind speed, E-CAPE may be calculated more accurately. A similar line of investigation may also contribute to improvement of cumulus parameterization used in the AGCM. Further investigation of entrainment rates of supercells and other convective clouds in environment with vertical wind shear will be important issues to be studied in future.

## **Acknowledgments**

I would like to sincerely thank Prof. Hiroshi Niino for his generosity and patience. I appreciate the examiners of this thesis, Professors Masaki Satoh, Kaoru Sato, Hiroyasu Hasumi, and Masahiro Watanabe. I particularly thank to Dr. Eigo Tochimoto for discussions about the analysis of this study. Special thanks to Prof. Keita Iga, Dr. Wataru Yanase, Dr. Shun-ichi Watanabe for their thoughtful comments. I am grateful to Dr. Junshi Ito and Sho Yokota for their suggestive comments. I also thanks to supports and joy by staffs and students at Department of Physical Oceanography, Atmosphere and Ocean Research Institute, The University of Tokyo.

Almost all figures were created by using the Grid Analysis and Display System (GrADS). The CM1 model is provided by Dr. George Bryan. The source code of the model can be downloaded from his webpage (<http://www2.mmm.ucar.edu/people/bryan/cm1/>).

I deeply thank my parents. I cannot write out this thesis without their help. I also thank to darling brother. I dedicate this thesis to them.

## References

- Arakawa, A., and W. H. Schubert, 1974: Interaction of a cumulus cloud ensemble with the large-scale environment, Part I. *J. Atmos. Sci.*, **31**, 674–701.
- Batchelor, G. K., 1954: Heat convection and buoyancy effects in fluids. *Quart. J. Roy. Meteor. Soc.*, **80**, 339–358.
- Brooks, H. E., C. A. Doswell III, and R. B. Wilhelmson, 1994: The role of midtropospheric winds in the evolution and maintenance of low-level mesocyclones. *Mon. Wea. Rev.*, **122**, 126–136.
- Browning, K. A., 1964: Airflow and precipitation trajectories within severe local storms which travel to the right of the winds. *J. Atmos. Sci.*, **21**, 634–639.
- Bryan, G. H., and J. M. Fritsch, 2002: A benchmark simulation for moist nonhydrostatic numerical models. *Mon. Wea. Rev.*, **130**, 2917–2928.
- Bryan, G. H., J. C. Wyngaard, and J. M. Fritsch, 2003: Resolution requirements for the simulation of deep moist convection. *Mon. Wea. Rev.*, **131**, 2394–2416.
- Bunkers, M. J., B. A. Klimowski, J. W. Zeitler, R. L. Thompson, and M. L. Weisman, 2000: Predicting supercell motion using a new hodograph technique. *Wea. Forecasting*, **15**, 61–79.
- Chikira, M., and M. Sugiyama, 2010: A cumulus parameterization with state-dependent entrainment rate. Part I: Description and sensitivity to temperature and humidity profiles. *J. Atmos. Sci.*, **67**, 2171–2193.

- Curtis, L., 2004: Midlevel dry intrusions as a factor in tornado outbreaks associated with landfalling tropical cyclones from the Atlantic and Gulf of Mexico. *Wea. Forecasting*, **19**, 411–427.
- Davies, J. M., 1993: Hourly helicity, instability, and EHI in forecasting supercell tornadoes. Preprints, *17th Conf. on Severe Local Storms*, St. Louis, MO, Amer. Meteor. Soc., 107–111.
- Davies-Jones, R. P., 1984: Streamwise vorticity: The origin of updraft rotation in supercell storms. *J. Atmos. Sci.*, **41**, 2991–3006.
- Davies-Jones, R. P., D. W. Burgess, and M. Foster, 1990: Test of helicity as a tornado forecast parameter. Preprints, *16th Conf. on Severe Local Storms*, Kananaskis Park, AB, CANADA, Amer. Meteor. Soc., 588–592.
- Davies-Jones, R. P., R. J. Trapp, and H. B. Bluestein, 2001: Tornadoes and tornadic storms. *Severe Convective Storms, Meteor. Monogr.*, No. 50, Amer. Meteor. Soc., 167–221.
- Deardorff, J. W., 1980: Stratocumulus-capped mixed layer derived from a three-dimensional model. *Bound.-Layer Meteor.*, **18**, 495–527.
- Evans, J. L., and R. E. Hart, 2003: Objective indicators of the life cycle evolution of extratropical transition for Atlantic tropical cyclones. *Mon. Wea. Rev.*, **131**, 909–925.

- Fiorino, M., 2002: Analysis and forecasts of tropical cyclones in the ECMWF 40-year reanalysis (ERA-40). Extended Abstract, *25th Conf. on Hurricanes and Tropical Meteorology*, San Diego, CA, Amer. Meteor. Soc., 261–264.
- Fujita, T. T., K. Watanabe, K. Tsuchiya, and M. Shimada, 1972: Typhoon-associated tornadoes in Japan and new evidence of suction vortices in a tornado near Tokyo. *J. Meteor. Soc. Japan*, **50**, 431–453.
- Gray, R. W., 1919: A tornado within a hurricane area. *Mon. Wea. Rev.*, **47**, 639–639.
- Gregory, D., 2001: Estimation of entrainment rate in simple models of convective clouds. *Quart. J. Roy. Meteor. Soc.*, **127**, 53–72.
- Hart, R. E., 2003: A cyclone phase space derived from thermal wind and thermal asymmetry. *Mon. Wea. Rev.*, **131**, 585–616.
- Hill, E. L., W. Malkin, and W. A. Schulz Jr., 1966: Tornadoes associated with cyclones of tropical origin-practical features. *J. Appl. Meteor.*, **5**, 745–763.
- Holton, J. R., 2004: *An Introduction to Dynamic Meteorology*, 4th ed. Academic Press, 535pp.
- Kain, J. S., S. J. Weiss, D. R. Bright, M. E. Baldwin, J. J. Levit, G. W. Carbin, C. S. Schwartz, M. L. Weisman, K. K. Droegemeier, D. B. Weber, and K. W. Thomas, 2008: Some practical considerations regarding horizontal resolution in the first generation of operational convection-allowing NWP. *Wea. Forecasting*, **23**, 931–952.

- Keys, R. G., 1981: Cubic convolution interpolation for digital image processing. *IEEE Transactions on Acoustics, Speech, and Signal Processing*, **29**, 1153–1160.
- Khairoutdinov, M., and D. Randall, 2006: High-resolution simulation of shallow-to-deep convection transition over land. *J. Atmos. Sci.*, **63**, 3421–3436.
- Klemp, J. B., 1987: Dynamics of tornadic thunderstorms. *Annu. Rev. Fluid Mech.*, **19**, 369–402.
- Klemp, J. B., and R. B. Wilhelmson, 1978a: The simulation of three-dimensional convective storm dynamics. *J. Atmos. Sci.*, **35**, 1070–1096.
- Klemp, J. B., and R. B. Wilhelmson, 1978b: Simulations of right- and left-moving storms produced through storm splitting. *J. Atmos. Sci.*, **35**, 1097–1110.
- Klemp, J. B., R. B. Wilhelmson, and P. S. Ray, 1981: Observed and numerically simulated structure of a mature supercell thunderstorm. *J. Atmos. Sci.*, **38**, 1558–1580.
- Kobayashi, S., Y. Ota, Y. Harada, A. Ebita, M. Moriya, H. Onoda, K. Onogi, H. Kamahori, C. Kobayashi, H. Endo, K. Miyaoka, and K. Takahashi, 2015: The JRA-55 reanalysis: General specifications and basic characteristics. *J. Meteor. Soc. Japan*, **93**, 5–48.
- Lemon, L. R., and C. A. Doswell III, 1979: Severe thunderstorm evolution and mesocyclone structure as related to tornadogenesis. *Mon. Wea. Rev.*, **107**, 1184–1197.

- Lilly, D. K., 1986: The structure, energetics and propagation of rotating convective storms. Part I: Energy exchange with the mean flow. *J. Atmos. Sci.*, **43**, 113–125.
- Lin, C., and A. Arakawa, 1997: The macroscopic entrainment processes of simulated cumulus ensemble. Part II: Testing the entraining-plume model. *J. Atmos. Sci.*, **54**, 1044–1053.
- Mashiko, W., 2016: A numerical study on the 6 May 2012 Tsukuba City supercell tornado. Part II: Mechanisms of tornadogenesis. *Mon. Wea. Rev.*, **144**, 3077–3098.
- Mashiko, W., H. Niino, and T. Kato, 2009: Numerical simulation of tornadogenesis in an outer-rainband minisupercell of Typhoon Shanshan on 17 September 2006. *Mon. Wea. Rev.*, **137**, 4238–4260.
- McCaul, E. W., Jr., 1987: Observations of the Hurricane “Danny” tornado outbreak of 16 August 1985. *Mon. Wea. Rev.*, **115**, 1206–1223.
- McCaul, E. W., Jr., 1991: Buoyancy and shear characteristics of hurricane-tornado environments. *Mon. Wea. Rev.*, **119**, 1954–1978.
- McCaul, E. W., Jr., and M. L. Weisman, 1996: Simulations of shallow supercell storms in landfalling hurricane environments. *Mon. Wea. Rev.*, **124**, 408–429.
- Mitchell, C. L., 1929: The tropical cyclone of September 18–October 4, 1929. *Mon. Wea. Rev.*, **57**, 418–420.

- Molinari, J., D. M. Romps, D. Vollaro, and L. Nguyen, 2012: CAPE in tropical cyclones. *J. Atmos. Sci.*, **69**, 2452–2463.
- Morrison, H., J. A. Curry, and V. I. Khvorostyanov, 2005: A new double-moment microphysics parameterization for application in cloud and climate models. part I: Description. *J. Atmos. Sci.*, **62**, 1665–1677.
- Morrison, H., G. Thompson, and V. Tatarskii, 2009: Impact of cloud microphysics on the development of trailing stratiform precipitation in a simulated squall line: Comparison of one- and two-moment schemes. *Mon. Wea. Rev.*, **137**, 991–1007.
- Niino, H., T. Fujitani, and N. Watanabe, 1997: A statistical study of tornadoes and waterspouts in Japan from 1961 to 1993. *J. Climate*, **10**, 1730–1752.
- Noda, A. T., and H. Niino, 2010: A numerical investigation of a supercell tornado: Genesis and vorticity budget. *J. Meteor. Soc. Japan*, **88**, 135–159.
- Novlan, D. J., and W. M. Gray, 1974: Hurricane-spawned tornadoes. *Mon. Wea. Rev.*, **102**, 476–488.
- Orton, R., 1970: Tornadoes associated with Hurricane Beulah on September 19–23, 1967. *Mon. Wea. Rev.*, **98**, 541–547.
- Romps, D. M., and Z. Kuang, 2010: Do undiluted convective plumes exist in the upper tropical troposphere? *J. Atmos. Sci.*, **67**, 468–484.
- Rotunno, R., and J. B. Klemp, 1982: The influence of the shear-induced pressure gradient on thunderstorm motion. *Mon. Wea. Rev.*, **110**, 136–151.

- Rotunno, R., and J. B. Klemp, 1985: On the rotation and propagation of simulated supercell thunderstorms. *J. Atmos. Sci.*, **42**, 271–292.
- Schenkman, A. D., M. Xue, and M. Hu, 2014: Tornadogenesis in a high-resolution simulation of the 8 May 2003 Oklahoma City supercell. *J. Atmos. Sci.* **71**, 130–154.
- Smith, J. S., 1965: The hurricane-tornado. *Mon. Wea. Rev.*, **93**, 453–459.
- Stommel, H., 1947: Entrainment of air into a cumulus cloud. *J. Meteor.*, **4**, 91–94.
- Stommel, H., 1951: Entrainment of air into a cumulus cloud II. *J. Meteor.*, **8**, 127–129.
- Suzuki, O., H. Niino, H. Ohno, and H. Nirasawa, 2000: Tornado-producing mini supercells associated with Typhoon 9019. *Mon. Wea. Rev.*, **128**, 1868–1882.
- Takishita, Y., 2009: Improvement of information about small-scale hazardous winds (in Japanese). *Tenki*, **56**, 167–175.
- Trapp, R. J., G. J. Stumpf, and K. L. Manross, 2005: A reassessment of the percentage of tornadic mesocyclones. *Wea. Forecasting*, **20**, 680–687.
- Vescio, M. D., S. J. Weiss, and F. P. Ostby, 1996: Tornadoes associated with Tropical Storm Beryl. *Natl. Wea. Dig.*, **21**, 2–10.
- Warner, J., 1955: The water content of cumuliform cloud. *Tellus*, **7**, 449–457.
- Warner, J., 1970: On steady-state one-dimensional models of cumulus convection. *J. Atmos. Sci.*, **27**, 1035–1040.

- Weisman, M. L., and J. B. Klemp, 1982: The dependence of numerically simulated convective storms on vertical wind shear and buoyancy. *Mon. Wea. Rev.*, **110**, 504–520.
- Wilhelmson, R. B., and J. B. Klemp, 1978: A numerical study of storm splitting that leads to long-lived storms. *J. Atmos. Sci.*, **35**, 1974–1986.
- Wilks, D. S., 2006: *Statistical Methods in the Atmospheric Sciences*, 2nd ed. Academic Press, 627pp.
- Yih, C. S., 1951: Free convection due to a point source of heat. *Proc. First U.S. Nat. Cong. Appl. Mech.*, p. 941.